40th AIAA/ASME/SAE/ASEE Joint Propulsion Conference and Exhibit
11 - 14 July 2004, Fort Lauderdale, Florida

40th AIAA/ASME/SAE/ASEE Joint Propulsion Conference
Fort Lauderdale, FL, July 11-14, 2004

AIAA-2004-3404

CFD Methods for Computing the Performance of Supersonic Inlets

John W. Slater*
NASA Glenn Research Center at Lewis Field, Brook Park, Ohio, 44135

Methods of computational fluid dynamics (CFD) are being used to analyze the airflow through supersonic inlets as an integral part of the design process. CFD is capable of providing inlet performance measures such as the amounts of engine-face flow, bleed, and spillage and engine-face quantities such as average Mach number, total pressure recovery, and total pressure distortion, as well as, flow properties and velocity components of the flow field. Essential to the analysis is the use of CFD methods that model turbulence, engine-face / outflow conditions, porous bleed, throat slot, and vortex generators. This paper discusses some lessons learned in applying such methods for the analysis of supersonic inlets.

Nomenclature

A_{cap}	=	capture area
A_{region}	=	area of a bleed region
α_{bleed}	=	angle-of-incidence of bleed holes
DPCPAV	=	average of ARP 1420 circumferential distortion descriptors of rings
M_{local}	=	Mach number at the edge of the boundary layer over a bleed region
$\dot{m}_{bleed}$	=	bleed mass flow rate
$\hat{n}$	=	unit normal vector
p_{plenum}	=	static pressure of a bleed plenum
p_t	=	total pressure
Φ	=	bleed region porosity
R	=	gas constant
Q_{sonic}	=	sonic flow coefficient
ρ	=	static density
γ	=	ratio of specific heats
T_t	=	total temperature
$\vec{u}_{bleed}$	=	velocity component
V_∞	=	freestream velocity
W_2	=	engine weight flow
W_{bleed}	=	bleed flow
W_{cap}	=	captured weight flow
$W_{spillage}$	=	spillage

I. Introduction

An inlet for a supersonic aircraft captures a portion of the freestream air flow and compresses it for intake by a gas turbine engine. This should be done efficiently while providing the engine with quality airflow. Two of the major concepts for supersonic inlet design are external-compression and mixed-compression inlets. An external-compression inlet performs its supersonic compression outside of the duct leading to the engine. A terminal normal shock is formed outside of the duct that results in the deceleration of the flow to subsonic speeds leading to the engine face. A mixed-compression inlet performs its supersonic compression outside and within the duct leading to the engine. The throat is the minimum area of the duct. The terminal normal shock is formed downstream of the

* Aerospace Engineer, Inlet Branch, 21000 Brookpark Rd / MS 86-7, Senior Member AIAA. This material is declared a work of the U.S. Government and is not subject to copyright protection in the United States..

This material is declared a work of the U.S. Government and is not subject to copyright protection in the United States.

throat. A mixed-compression inlet holds the promise of greater aerodynamic performance than an external-compression inlet; however, at the cost of less flow stability and greater mechanical complexity and weight.

The NASA Glenn Research Center has been active in the design and analysis of supersonic inlets for over 50 years. References 1 through 6 provide just a sample of some of the past research efforts. The focus has been on aircraft capable of cruising within the range of Mach 1.5 to 3.5 and has included inlet concepts using external-compression and mixed-compression. The latest effort has focused on the Parametric Inlet, which is an advanced external-compression inlet which approaches the performance of a mixed-compression inlet but with less mechanical complexity.[7] Figure 1 shows the Parametric Inlet mounted in the NASA Glenn Research Center 10-foot-by-10-foot supersonic wind tunnel. The "parametric" aspect involved options for various cowl, slot, and sidewall configurations.

The design of the Parametric Inlet relied heavily on computational fluid dynamics (CFD) to examine the aerodynamic performance of the inlet. Figure 1 shows the computational geometry model used in some of the CFD simulations. Due to geometric and flow symmetry, only half of the inlet needed to be modeled.

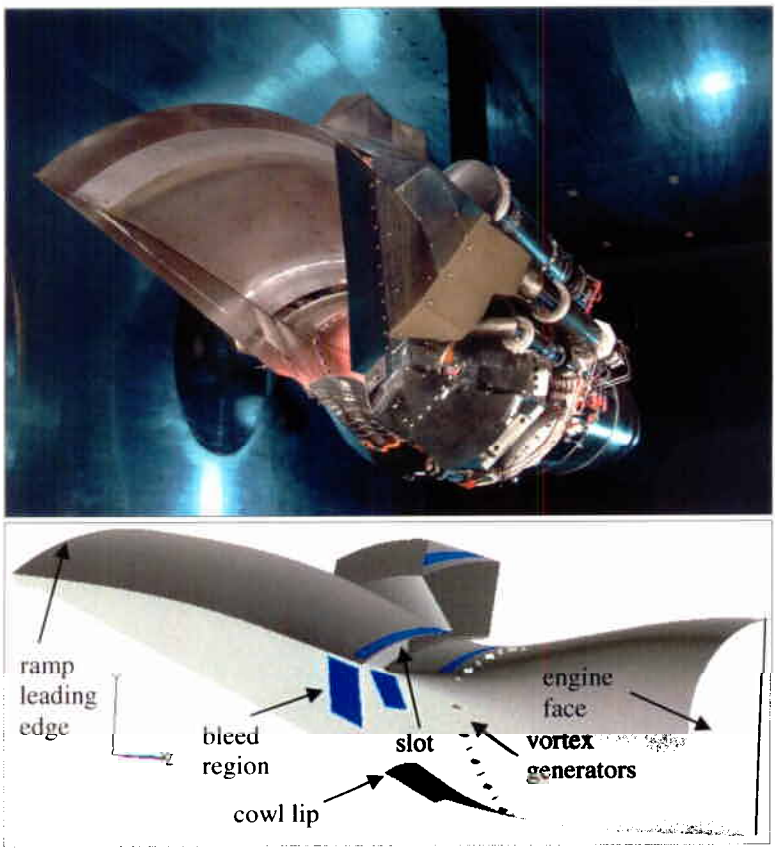

Figure 1. The Parametric Inlet in the NASA Glenn 10-ft-by-10-ft supersonic wind tunnel (top) and as a computational geometry model for CFD simulations (bottom).

The simulation of the flow through a supersonic inlet requires an understanding of the type of flow expected within the inlet. The transition from supersonic to subsonic flow involves oblique and normal shocks waves which interact with turbulent boundary layers on the inlet surfaces. The inlet is a compression device, and so, an adverse pressure gradient exists throughout the flow. The diffusion of the flow and the positioning of the engine axis will require significant turning of the flow at transonic speeds. This all leads to the possibility of boundary layer separation and flow reversal on regions of the inlet surfaces. Such flow features result in a decrease in the performance of the inlet. A CFD simulation must accurately capture these flow features. Figure 2 shows the Mach number contours on the symmetry plane of the Parametric Inlet. The freestream Mach number is 2.35. An oblique shock forms at the leading edge of the compression ramp and extends to below the cowl where it intersects the cowl shock. The cowl shock merges with the terminal shock which extends to interact with the slot. The compression

ramp is characterized by decreasing Mach number and increasing boundary layer thickness. The slot plenum contains low subsonic flow. The flow is subsonic downstream of the terminal shock. The boundary layer at the top of the subsonic diffuser contains some boundary layer separation.

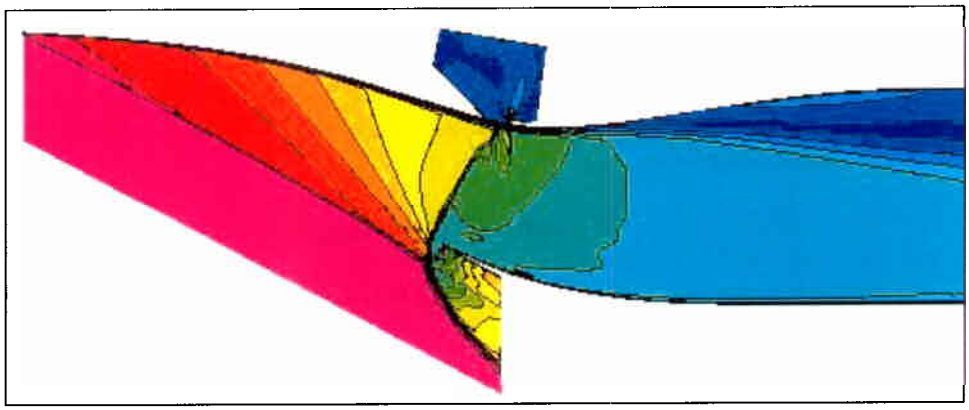

Figure 2. Mach number contours of the flow through the Parametric Inlet.

In the past, the design and development of supersonic inlets has relied on techniques such as method of characteristics, boundary layer analysis, and planar computational fluid dynamic (CFD) analyses for sizing, layout, and preliminary design. The inlet was then fabricated and then put through an extensive wind tunnel test matrix to determine the inlet configuration that provided the best performance. At the present, CFD methods are now capable of simulating the three-dimensional turbulent flow about the complex shape of the inlets. Further, they are being used as part of the design process and contribute significantly to the development of the design. For the Parametric Inlet design, CFD simulations were used to demonstrate the overall performance of the inlet, highlight flow problems, and recommend fixes prior to and during fabrication. CFD analysis was also used to study bleed configurations and rates and parameters for the cowl lip and throat slot configurations prior to wind tunnel testing. CFD was used to improve the design and make effective use of expensive wind tunnel resources.

The performance of a supersonic inlet is characterized by several performance measures involving airflow quantities and several involving engine-face quantities. The performance measures involving airflow quantities are the engine weight flow, bleed flow, and spillage. The performance measures involving engine-face quantities are the average Mach number, total pressure recovery, and total pressure distortion at the engine face. These performance measures will be discussed in detail in a later section.

A CFD code used for the simulation of the flow through a supersonic inlet must contain several methods to accurately model and simulate the flow through a supersonic inlet. These include models for turbulence, engine-face / outflow, porous bleed, throat slot, and vortex generators. The methods for each of these models will be discussed in a later section. The CFD code used for the simulations discussed in this paper was the Wind-US CFD code of the NPARC Alliance.

The purpose of this paper is to discuss the specific CFD methods that are critical for the CFD analysis of a supersonic inlet. While the Parametric Inlet is used as an example, specific information as to the performance of the Parametric Inlet, experimental procedures and results, and comparison of CFD results to the experimental data will be topics of future papers.

II. Wind-US CFD Code

The inlet aerodynamic simulations were performed using the Wind-US CFD code. Wind-US is being developed by the NPARC Alliance (National Program for Applications-oriented Research in CFD), which is an alliance of the NASA Glenn Research Center, the Air Force Arnold Engineering Development Center, and the Boeing Company.[8-10] Wind-US solves the time-dependent, Reynolds-averaged Navier-Stokes equations for turbulent, compressible flows using a cell-vertex, finite-volume, time-marching approach. The inlet analyses were performed using multi-zone, structured grids. Spatial accuracy is formally second-order using the Roe flux-difference splitting upwind formulation. Steady flows are simulated through an iterative process using local time stepping. Turbulence is modeled using algebraic, one-equation, or two-equation eddy viscosity models. Wind-US is capable of solving for flows of speeds ranging from low subsonic to hypersonic. High-temperature effects of airflow can be modeled with Wind-US; however, supersonic inlet simulations used the calorically perfect gas model.

III. Inlet Performance Measures

The inlet performance can be characterized by airflow performance measures and engine-face performance measures.

The airflow performance measures include engine weight flow (W_2), bleed flow (W_{bleed}), and spillage ($W_{spillage}$). The engine weight flow (W_2) is the amount of flow that goes through the engine face. The bleed flow (W_{bleed}) is the amount of flow that is removed through the slot or porous bleed regions. The engine weight flow and the bleed flow can both be computed accurately from the CFD flow field solution. The spillage ($W_{spillage}$) is the amount of flow that escapes past the sidewalls or over the cowl lip, and so, is lost to the inlet. The engine weight flow, bleed flow, and spillage form a mass balance of the form

$$W_{cap} = W_2 + W_{bleed} + W_{spillage} \tag{1}$$

where W_{cap} is the captured weight flow. The captured weight flow is the amount of flow the inlet would "capture" under ideal circumstances. It is defined here as

$$W_{cap} = \rho_\infty V_\infty A_{cap} \tag{2}$$

where A_{cap} is the capture area representing the frontal planar opening of the inlet. For the Parametric Inlet, a reference capture area was defined and held fixed throughout the design. Thus, from Eq. 2, the captured weight flow becomes a fixed reference value throughout the design. The spillage ($W_{spillage}$) can then be determined from Eq. 1. The spillage can be separated into supersonic spillage occurring before the terminal shock and subsonic spillage occurring past the cowl lip; however, exactly determining these two amounts is difficult.

The engine-face performance measures include average Mach number (M_2), total pressure recovery, and total pressure distortion (DPCPAV). The engine-face is planar and typically circular. The average Mach number is the average over the engine-face. The total pressure recovery measures the amount of energy loss of the flow stream as it moves from the freestream ahead of the inlet through the inlet to the engine face. The total pressure recovery is computed as the ratio of the average total pressure at the engine face to the total pressure of the freestream flow. Averages can be with respect to the mass flowing through the engine face (mass-averaged) or to the area of the engine face (area-averaged). The total pressure distortion measures the variation of the total pressure over the engine face. Ideally, one desires uniform flow field over the engine face. A non-uniform flow presents the engine with varying flow conditions, which can reduce engine performance, cause instabilities in the engine, and result is increased fatigue of the engine components. Of special interest is distortion in the circumferential direction, which is the direction of rotation of the gas turbine engine.

A standard procedure for representing the total pressure field at a circular engine face is outlined in the SAE ARP (Aerospace Recommended Practice) 1420, which contains a 40-probe rake consisting of 8 radial arms with 5 concentric rings.[11] Each total pressure probe is located at the centroid of equal-area sections of the engine face area. Thus, the total pressure of each probe represents the area-average of that equal-area section. The average of the 40 total pressure values represents the area-averaged total pressure of the engine face. The total pressure recovery is simply the ratio of the area-averaged total pressure at the engine face to the freestream total pressure. The ARP 1420 also outlines methods for computing circumferential distortion intensity descriptors for each ring (ΔPC/P). An engine-face measure of total pressure distortion (DPCPAV) can be obtained by a simple average of the distortion intensity descriptors (ΔPC/P) of all the rings. In a CFD simulation, the flow field can be interpolated onto the location of the rake probes. Alternatively, the total pressure can be integrated numerically based on the CFD grid at the engine face.

Figure 3 shows plots of these performance measures as determined from CFD simulations of the Parametric Inlet. The labels for the plots can not be shown at this time since the official reports on the Parametric Inlet have not been released. The captions do provide some idea of the scale of variation between tick marks. The point of the plots is to provide an example of the variations of these performance measures.

An inlet is usually designed for a specific flow condition, but it must also have good performance for a range of flow conditions as characterized by the engine weight flow (W_2). The plots of Fig. 3 show the performance measures with respect to the engine weight flow normalized by the captured weight flow (W_{cap}). The plot of the total pressure recovery with respect to the engine weight flow is known as the "mass flow cane curve" because it is characterized by a near level or peak value of recovery at the engine design weight flows and then a sudden drop in recovery at higher engine weight flows. At an engine weight flow below the design point, the flow can become

unstable, causing duct rumble or "buzz" for an external compression inlet. The "buzz" is due to unsteady shock / boundary layer interactions and movement of the terminal shock on the external compression ramp. The "knee" in the cane represents the desired operating point of the inlet since recovery is near maximum while engine weight flow is maximized (conversely, the bleed and spillage are lower). This ensuring that the engine design flow occurs at the best inlet recovery is commonly referred to as inlet-engine matching and allows the propulsion designer to "size" the inlet. At the higher engine weight flows, the terminal shock moves downstream and further into the subsonic diffuser. The shock / boundary layer interactions result in separated boundary layers that result in a drop in the total pressure recovery and an increase in the average Mach number and total pressure distortion at the engine face. The amount of bleed flow decreases since more of the bleed regions are upstream of the terminal shock. The spillage decreases slightly to reach the value of the supersonic spillage.

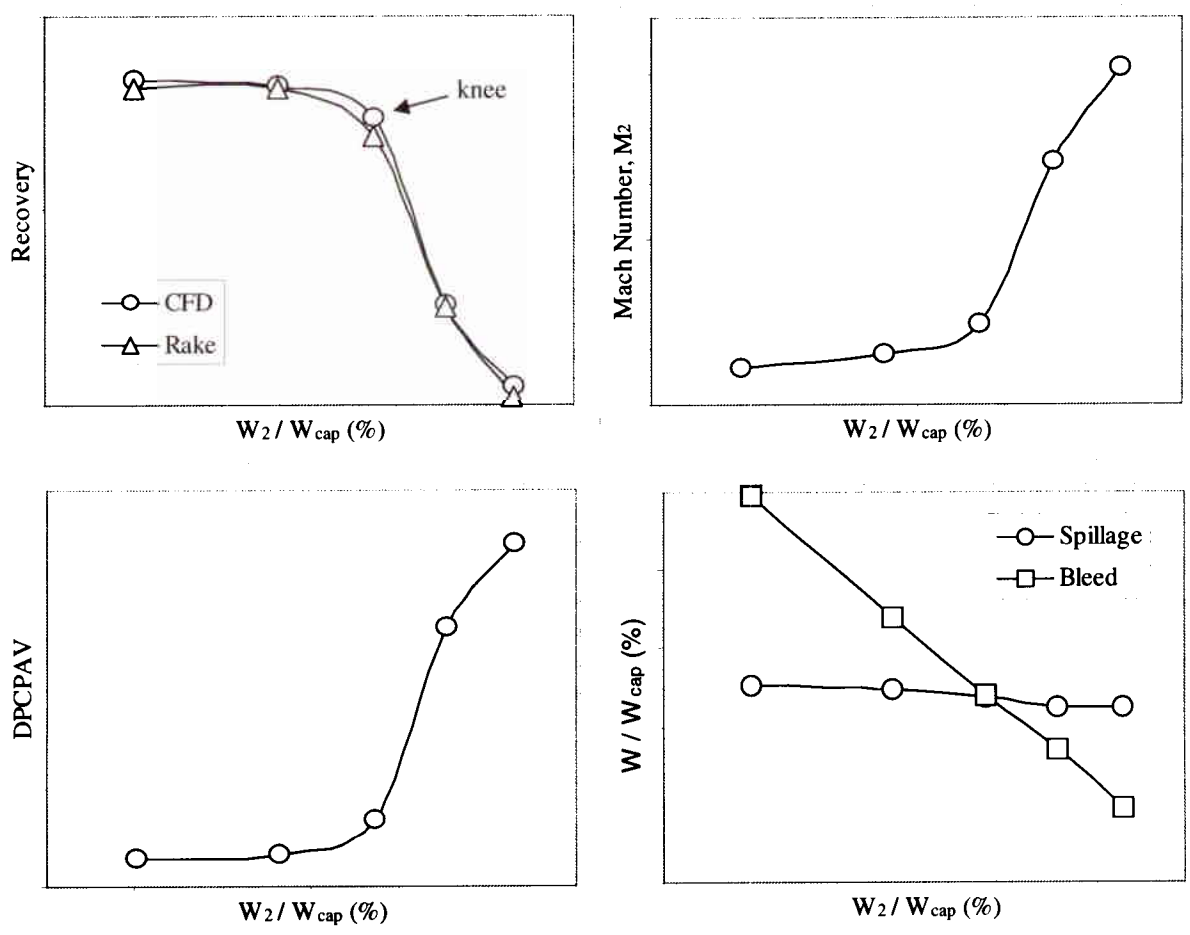

Figure 3. Performance plots from CFD simulations: mass flow cane curve (top-left), average engine-face Mach number (top-right), average circumferential distortion (bottom-left), and spillage and bleed flows (bottom-right). Tick marks of horizontal axis represent 2% of W_{cap}. Tick marks of vertical axis represent 4% of recovery, 0.05 of M_2, 0.05 of DPCPAV, and 2% of W_{cap}, respectively.

IV. Turbulence Modeling

The supersonic speeds of the flow and the relatively large scale of a supersonic inlet suggest that the flow is fully turbulent, except possibly a small region at the start of the external compression ramp.[12] The presence of shocks and an adverse pressure gradient also encourage turbulent flow. A CFD simulation of such flows thus requires accurate modeling of turbulence. Wind-US has several options for modeling turbulence, including algebraic, one-equation, and two-equation turbulence models.[8,13] The level of turbulence and the presence of boundary layer separation require the use of at least a one-equation model. The Spalart-Allmaras (S-A) model is the primary one-equation

model.[14] The SST model is the primary two-equation model.[15] Both models were developed for external flows; however, they have been successfully used for internal flows.

Both the S-A and SST turbulence models are low Reynolds number models in that they compute the turbulent viscosity through the inner region of a turbulent boundary layer. This requires the grid to resolve the inner region. The grid is clustered along the surfaces such that the y^+ distance for the first point off the surface was no more than $y^+ \sim 1\text{-}2$. A critical parameter in the grid quality for proper resolution and accurate computation of the boundary layer flow is the grid spacing ratio of the grid away from the surface. This is the ratio of grid spacing between adjacent grid points. A grid spacing ratio of 1.2 is a good value. Smoothly expanding the grid spacing from the wall has also been shown to help iterative convergence.

Both the S-A and SST turbulence models in Wind-US allow the use of the White-Christoph law of the wall function as a boundary condition at viscous surfaces.[16] The law of the wall computes the velocity distribution of an attached boundary layer in the inner region. Thus, grid points are not needed in this region, which reduces the size of the grid. Further, removing the smallest grid cells also increases the minimum local time step of the simulation, and so, results in faster iterative convergence. Reference 16 recommends that the grid be first generated as to resolve the flow through the inner region and then use some means to remove those grid point within the inner region to y^+ values of approximately 30 to 100. While technically one can not use a wall function in regions of separated flow, wall functions have been used in such flows with success. In the CFD analysis of the Parametric Inlet, the wall function was used for some initial simulations; however, it was decided not to use the wall function to remove possible sources of inaccuracy in the large regions of separation that were present.

The flow simulations were all steady-flow simulations using a Reynolds-averaging approach. The simulations only compute the time-average or mean turbulence, and so, small-scale unsteadiness is averaged out. However, large-scale unsteadiness (i.e. inlet unstart) can be picked up with the simulations. Wind-US also contains a hybrid turbulence model capability in which spatial limiting is applied to the Spalart-Allmaras and SST turbulence models to add large-eddy simulation (LES) modeling. Reference 17 suggests that using Wind-US with the SST / LESb model to compute the unsteady flow in a transonic inlet allows more accurate computation of the steady-state total pressure distortion. While this adds considerable more computational effort, it should be a consideration for future CFD analysis of inlets.

The choice of which turbulence model to use and which results can be trusted can be made easier by examining the sensitivity of the models. This requires conducting simulations with both models and comparing the results. Each model has its historical strengths and weaknesses, but behavior is dependent on the specific application. In a new application such as for the Parametric Inlet, uncertainties of the turbulence models are unknown. Figure 4 shows the mass flow cane curves for simulations with each model. Figure 5 shows the total pressure contours at the engine face. Both models show similar results. Other simulations showed some inconsistencies with the SST model that led to the decision to use the S-A model for the majority of the Parametric Inlet simulations.

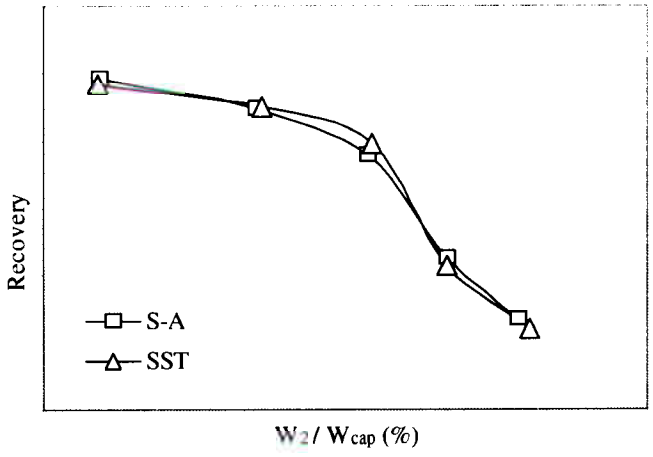

Figure 4. The sensitivity of the mass flow cane curve with respect to the choice of turbulence model. Tick marks represent 2% of W_{cap} and 5% of recovery.

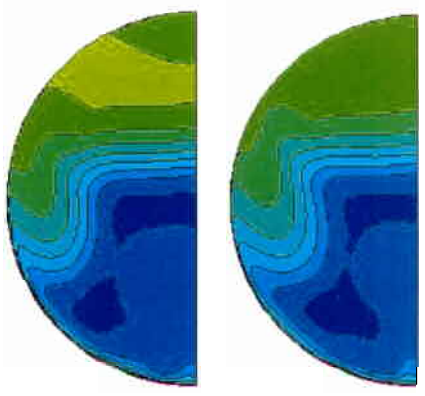

Figure 5. Total pressure contours at the engine face for the CFD simulations using the S-A (left) and SST (right) turbulence models.

V. Engine-Face / Outflow Modeling

The subsonic flow from an inlet leads to the engine face of a gas turbine engine. Rather than include the engine components in the CFD simulation, a boundary condition is applied at the outflow of the inlet. The characteristic nature of the flow at a subsonic outflow boundary indicates that one physical boundary condition can be applied. Several approaches exist for applying the boundary condition; however, the approaches essentially set the static pressure as the physical boundary condition. The choice of the approach becomes critical for supersonic inlet CFD simulations because establishing the terminal shock with subsonic flow in the subsonic diffuser can be difficult. In an internal, compressible flow, the propagation of acoustic waves in the subsonic diffuser during the early stages of an iterative convergence process can cause significant flow instability. A common practice is to move the outflow boundary of the flow domain downstream of the engine face so that the boundary condition has minimal impact on the local flow field near the engine face. This extension is typically a straight section of approximately two to three engine-face diameters in length and is known as an "isolator".

The first approach is to directly specify the static pressure at the engine face. A constant and uniform value of static pressure results in a very reflective boundary for acoustic waves. Acoustic waves can only propagate forward, and so, cause significant forward movement of the terminal shock onto the ramp. The static pressure could be allowed to vary spatially and with iterations, which reduces the reflective behavior of the boundary condition.

The second approach is to specify the amount of mass flow at the engine face. This can be the actual or the corrected mass flow. The corrected mass flow is adjusted to standard atmospheric pressure and temperature and becomes a function of only the engine face Mach number. This approach computes the static pressure at the boundary using an iterative method that adjusts the local static pressure until the engine-face mass flow approaches the specified mass flow. Specifying the mass flow makes it easier to perform simulations to generate the performance plots. About five simulations over a range of mass flows are required to adequately define the mass flow cane curve and other plots shown in Fig. 3.

A third approach is to attach a converging-diverging nozzle to the end of the isolator. A grid must be generated for the nozzle. Figure 6 shows the outline of the flow domain and grid zones of the Parametric Inlet with the zone in the upper right corner being the isolator and nozzle. The nozzle is operated to be choked. The supersonic outflow of the nozzle allows for a simple extrapolation boundary condition to be used. This approach has been found to be very non-reflective. Varying the radius of the nozzle throat varies the amount of static pressure at the compressor face station. For the example of the Parametric Inlet, the subsonic flow in the subsonic diffuser was established by opening the nozzle radius to almost the engine-face radius and initializing the flow through the inlet to be supersonic. The radius of the nozzle was reduced in gradual increments over several thousands of iterations. The nozzle eventually choked and a normal shock was formed in the subsonic diffuser. This shock moved upstream and eventually joined the cowl lip shock to form the terminal shock. Once the subsonic flow was established, a series of simulations are performed with various nozzle radii to construct a mass flow cane curve.

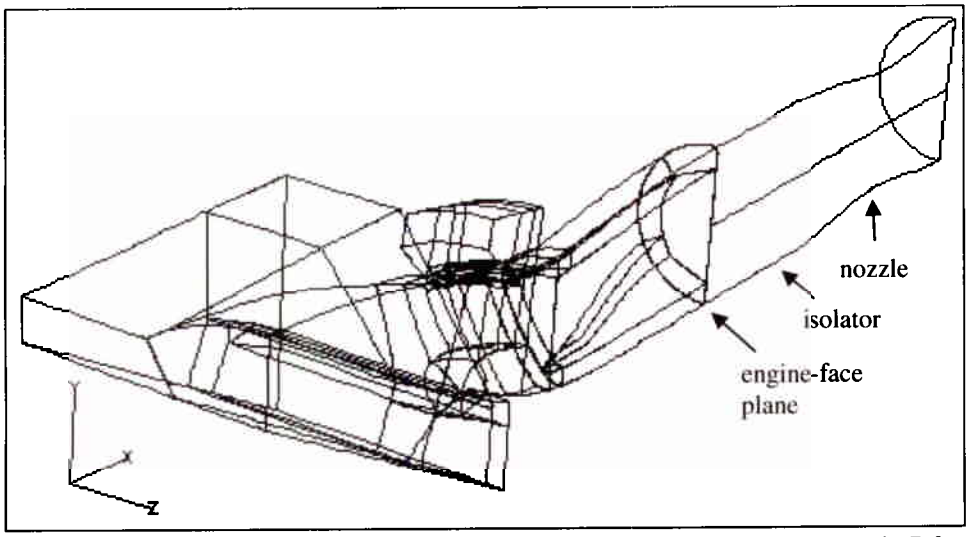

Figure 6. The outline of the flow domain and grid zones for the Parametric Inlet with an isolator and nozzle zone (upper right corner) attached to engine-face outflow plane.

VI. Porous Bleed Modeling

Porous bleed consists of small holes that are arranged in a pattern over a region of the surface of the inlet. Figure 7 shows the porous bleed regions used for the Parametric Inlet. Forward bleed regions are typically stability bleed regions for the normal terminal shock. The bleed regions in the throat are performance bleed regions designed to control excessive separation at boundary layer / shock interactions and transonic flow turning. The bleed holes lead to a plenum chamber connected to ducting through which the bleed flow exits. By adjusting the static pressure of the plenum, one controls the amount of low-energy boundary layer flow removed.

The porous bleed model is applied as a boundary condition on the surface of the inlet. An example of how the bleed region is defined is shown in Fig. 8. A "dummy" grid zone that has the outline of the bleed region is coupled to the inlet grid zone containing the surfaces encompassing the bleed region. The boundary condition utility is then able to change the "coupled" boundary grid points to bleed boundary conditions.

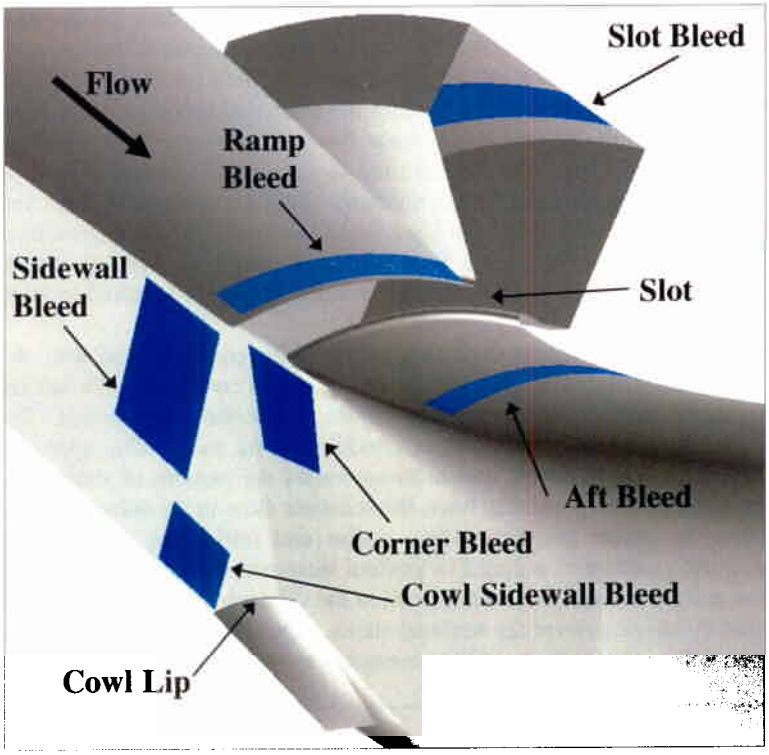

Figure 7. The bleed regions of the Parametric Inlet.

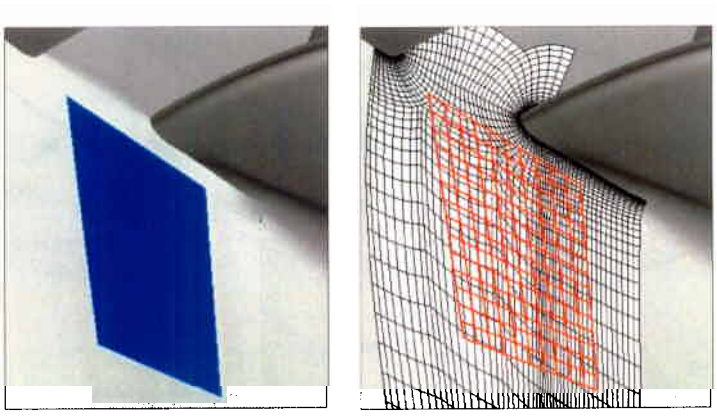

Figure 8. A porous bleed region and the grid used to set the boundary conditions.

The model for porous bleed relates the mass flow through the bleed to the normal velocity at the boundary,

$$\vec{u}_{bleed} = -\frac{\dot{m}_{bleed}}{\rho A_{region}} \hat{n} \tag{3}$$

where $\hat{n}$ is the boundary normal surface vector, which is directed into the flow domain. The ρ is the density and A_{region} is the area of the bleed region. One option is to directly specify the bleed mass flow; however, this does not accurately represent actual bleed hole behavior, especially in the presence of spatially varying shock waves in the bleed regions. The bleed mass flow should vary according to local flow conditions. One model is

$$\dot{m}_{bleed} = Q_{sonic}\, p_t\, \Phi\, A_{region} \left(\frac{\gamma}{RT_t}\right)^{1/2} \left(1+\frac{\gamma-1}{2}\right)^{-[(\gamma+1)/2(\gamma-1)]} \tag{4}$$

where p_t and T_t are the local total pressure and total temperature, respectively.[18] The γ and R are the ratio of specific heats and gas constant, respectively. The Φ is the porosity of the bleed region, which is the ratio of the total hole area to A_{region}. A typical porosity is about 40%. The Q_{sonic} is the sonic flow coefficient that is the ratio of the bleed mass flow to the maximum bleed flow, which occurs with sonic flow through the bleed hole. The Q_{sonic} is determined from an empirical model of the form

$$Q_{sonic} = f\left(\alpha_{bleed}, M_{local}, \frac{p_{plenum}}{p_t}\right) \tag{5}$$

where α_{bleed} is the angle of the bleed hole with respect to the inlet surface. The M_{local} and p_t are the Mach number and total pressure at the edge of the boundary layer above the bleed hole. The p_{plenum} is the static pressure of the bleed plenum. Thus, the independent variable in the model is p_{plenum}. Reference 19 discusses further features of this bleed model with respect to shock waves and supersonic inlets.

Figure 9 shows the effect of bleed on the mass flow cane curve for simulations of the Parametric Inlet. At the lower engine weight flows, the terminal shock sits forward of the cowl lip and ahead of most of the bleed regions. The stability bleed regions operate to allow for stable operation of the inlet. Figure 10 illustrates the interaction of the cowl shock with a bleed region near the cowl lip. As the engine weight flow is reduced, the cowl shock is pushed forward, resulting in a greater pressure on the bleed region, which causes a higher bleed flow. The high-pressure air downstream of the terminal shock also causes a greater amount of bleed. As the engine weight flow increases, the shock moves more into the inlet and downstream of the bleed regions. This reduces the bleed to nearly zero flow, which is indicated by the similarity of the two curves of Fig. 9 at the higher engine weight flows. Figure 11 provides an accounting of the bleed flows of each of the performance bleed regions. As can be seen, the slot extracts the most bleed over the range of engine weight flows and shows the greatest variation. At the higher engine weight flows, the slot is essentially turned off by the bleed model. This is what should occur since the terminal shock is downstream of the slot at this point.

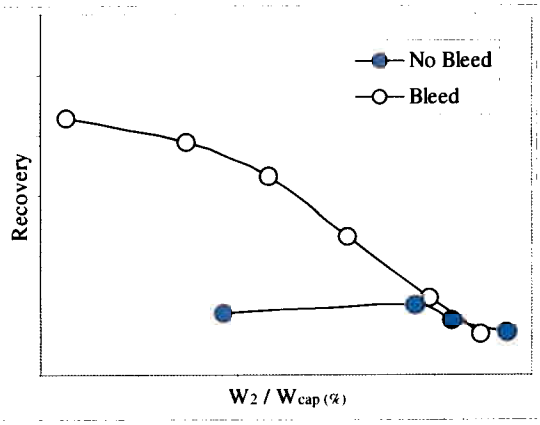

Figure 9. The effect of bleed on the inlet mass flow cane curve. Each tick mark span represents 2% of W_{cap} and 5% of recovery.

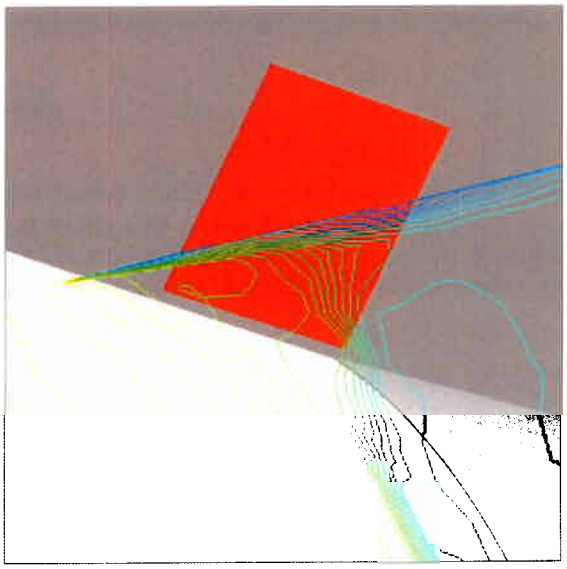

Figure 10. The Mach number contours in the region of a porous bleed region on the sidewall.

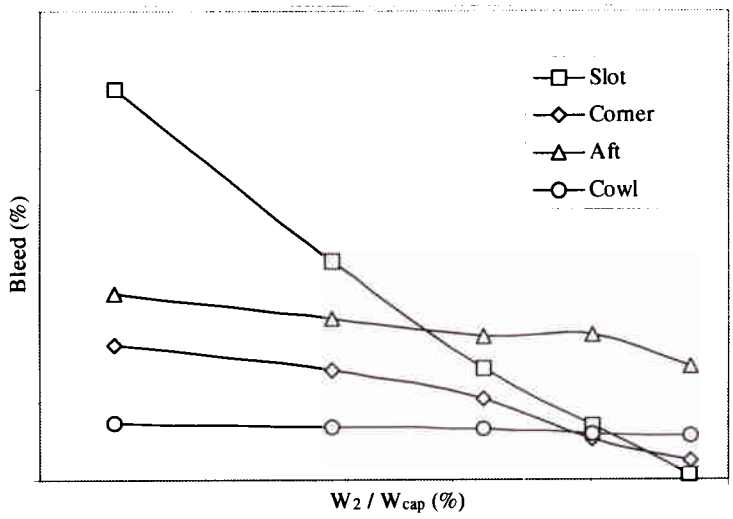

Figure 11. The variation of the bleed rates over each bleed region with various engine weight flows. Each tick mark span represents 2% of W_{cap} and 1% of W_{bleed}.

VII. Throat Slot Modeling

The throat slot is an important design feature for a supersonic inlet in that it reduces adverse effects of the interactions of the terminal shock with the turbulent boundary layer as the flow is turning into the subsonic diffuser. The slot opens into a plenum. A slight bleed of the flow through the slot helps to turn the main inlet flow. However, a slot introduces complexity into the geometric modeling and grid generation of a CFD analysis. Figure 12 shows the outline shape and grid for the throat slot at the mid-plane of the Parametric Inlet. The trailing and leading edges of the slot are elliptic to help the air flow into the slot plenum. Two approaches were examined for modeling the slot. The first approach was to assume a faired surface over the slot opening that resulted in a smooth surface for the flow from the supersonic ramp to the subsonic diffuser. A bleed region was specified on this surface in place of the slot. The second approach was to model the geometry of the slot and generate a grid. The actual slot plenum was quite complex, and so, a simplified plenum geometry was assumed. A bleed region was specified at the

top of the slot plenum to remove a portion of the flow. The second approach was found to be almost required to realistically simulate the behavior of the inlet flow in the throat region, and so, accurately compute the performance of the inlet. The first approach with a bleed region did not sufficiently capture the correct interaction between the terminal shock and the slot. The first approach yielded a boundary layer in the slot region, while the second approach allowed a shear layer between the main inlet flow and the slot plenum, which is what is actually present in the inlet flow.

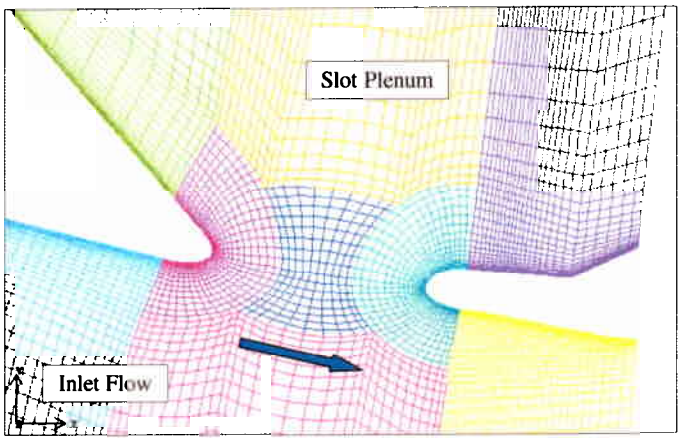

Figure 12. The geometry and grid about the throat slot.

VIII. Vortex Generator Modeling

Vortex generators are small airfoil-shaped tabs that are placed at an incidence to the flow and generate a vortex that energizes the boundary layer and helps to limit boundary layer separation. Three approaches to modeling vortex generators are possible with Wind-US. The first approach is to model the actual airfoil geometry of each vortex generator and generate a grid. The second approach is to model each vortex generator as a flat plate with the same span, chord length, and angle-of-incidence as the airfoil shape. This simplifies the grid generation and significantly reduces the number of grid points required. A third approach is to use a vortex generator model that uses an empirical relation to place a vortex in the flow field. The third approach was still under development at the time of this study, and so, results using the empirical vortex generator model are not discussed here.

To examine the first two approaches for modeling the vortex generators, a study was conducted with an isolated vortex generator in a rectangular duct. The shape of the vortex generator was based on the NACA 0012 airfoil. The angle-of-incidence of the vortex generator was 16 degrees. Figure 13 shows the two grids generated about the vortex generator. The image on the left shows the vortex generator in which the actual airfoil shape was modeled. The image on the right shows the vortex generator modeled as a flat plate. Simulations were performed with the same flow conditions. Figure 14 shows the flow field in a region local to the vortex generator. As can be seen in the Mach contours of the flat plate, there is considerable boundary layer separation on the upper surface of the plate; however, away from the vortex generator the Mach contours look similar to those of the airfoil shape. For an inlet simulation, the important result is what happens to the flow downstream at the engine face. Figure 15 shows the Mach contours at the engine face location. The two contour plots are very similar. This suggests that as long as one is not too interested in the flow local to the vortex generator, modeling the vortex generator as a flat plate provides sufficient modeling of the vortex generators with less complex grids and less computational effort than the first approach.

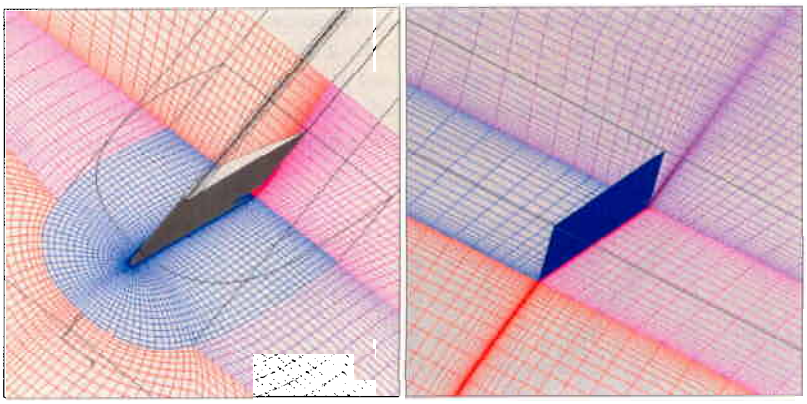

Figure 13. The grids about a vortex generator modeled as an airfoil (left) and a flat plate (right).

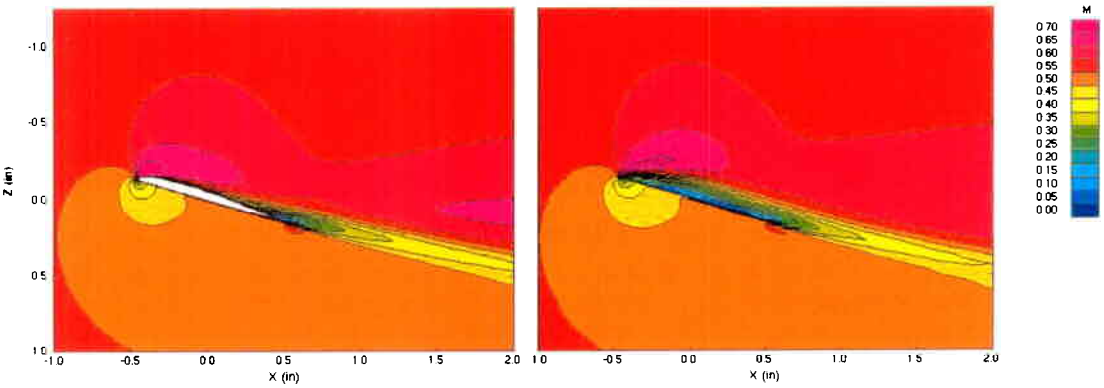

Figure 14. The Mach number contours in the area near the vortex generators modeled as an airfoil (left) and a flat plate (right).

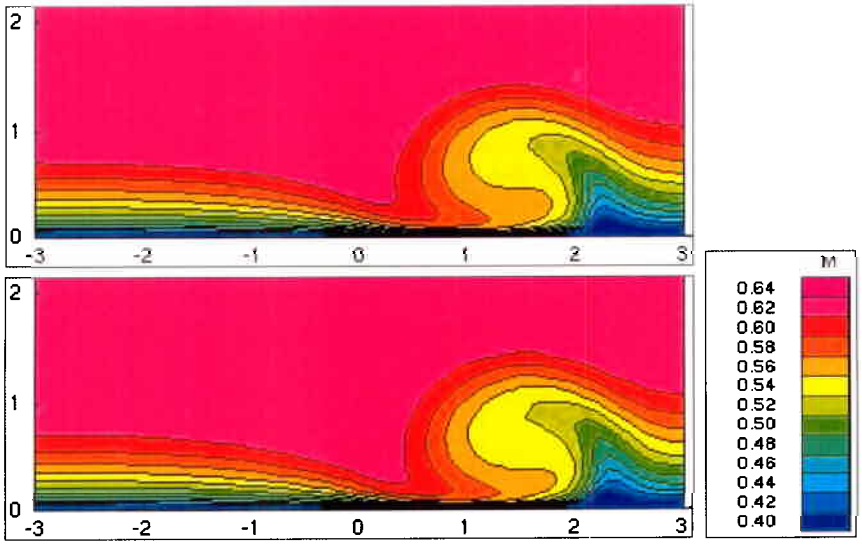

Figure 15. The Mach number contours in the cross-plane at an axial station 25 chord lengths downstream of the vortex generators modeled as an airfoil (top) and flat plate (bottom).

In the example of the Parametric Inlet, there was a single row of vortex generators in the subsonic diffuser. Figure 1 shows their approximate location and an example configuration involving counter-rotating pairs of vortex generators. The vortex generators are modeled as flat plates to simplify the grid generation. Simulations were performed with and without the vortex generators. Figure 16 shows the mass flow cane curves for the CFD simulations. The plots show that at lower engine flows, the vortex generators reduce the recovery – they essentially act as drag devices. At the higher engine flows, the vortex generators are enveloped in a region of separated flow, and so, are not positioned correctly to be effective in improving recovery. Figure 17 shows the total pressure contours at the engine face. The vortex generators are effective in redistributing the total pressure. The DPCPAV distortion measure decreases approximately 14% with use of the vortex generators.

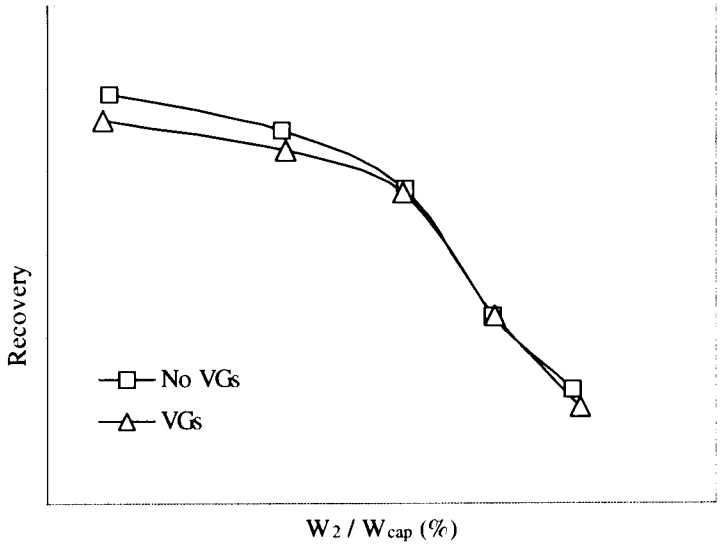

Figure 16. The effect of vortex generators on the mass flow cane curve for the Parametric Inlet.

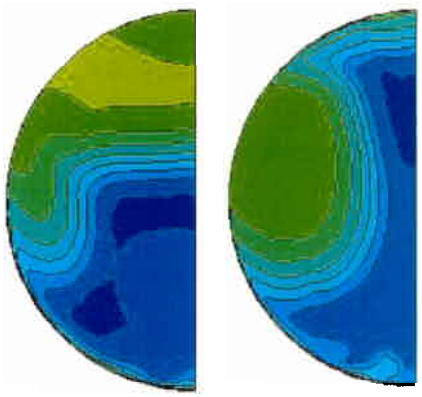

Figure 17. The total pressure contours at the engine face for the CFD simulations without vortex generators (left) and with vortex generators (right).

IX. Summary and Conclusions

CFD methods for modeling turbulence, engine-face / outflow, porous bleed, slots, and vortex generators were discussed as to their importance for the simulation of flows through supersonic inlets. The example of the CFD simulations of the Parametric Inlet illustrated the importance of these methods in providing realistic estimates of the inlet performance.

References

[1]Esenwein, F.T. and A.S. Valerino, "Force and Pressure Characteristics for a Series of Nose Inlets at Mach Numbers from 1.59 to 1.99. I: Conical-Spike All-External-Compression Inlet with Subsonic Cowl Lip", NACA RM E50J26, January 1951.

[2]Anderson, B.H. and H.N. Bowditch, "Investigation of Inlet Control Parameters for an External-Internal-Compression Inlet from Mach 2.1 to 3.0", NACA RM E58G08, September 1958.

[3]Sanders, B.W. and G.A. Mitchell, "Increasing the Stable Operating Range of a Mach 2.5 Inlet", NASA TM X-52799, June 1970.

[4]Wasserbauer, J.F., R.J. Shaw, and H.E. Neumann, "Design of a Very-Low-Bleed Mach 2.5 Mixed-Compression Inlet with 45 Percent Internal Contraction," NASA TM X-3135, 1974.

[5]J.F. Wasserbauer, E.T. Meleason, and P.L. Burstadt, "Experimental Investigation of the Performance of a Mach-2.7 Two-Dimensional Bifurcated Duct Inlet With 30 Percent Internal Contraction", NASA TM-106728, May 1996.

[6]Saunders, J.D. and R. Girvin, "VDC Inlet Experimental Results," First NASA/Industry High Speed Research Propulsion/Airframe Integration Workshop, October 1993.

[7]Kandebo, S.W., "Improved Inlet", *Aviation Week and Space Technology*, May 24, 2004, p. 31.

[8]NPARC Alliance, "The Wind-US Code", URL: http://www.grc.nasa.gov/www/Wind-US_docs [cited 13 June 2004].

[9]Bush, R.H., G.D. Power, and C.E. Towne, "Wind-US: The Production Flow Solver of the NPARC Alliance", AIAA-1998-0935, January 1998.

[10]Mani, M., A. Cary, and S. Ramakrishnan, "A Structured and Hybrid-unstructured Grid Euler and Navier-Stokes Solver for General Geometry", AIAA-2004-0524, January 2004.

[11]Society of Automotive Engineers, "Gas Turbine Engine Inlet Flow Distortion Guidelines", SAE ARP 1420, February 2002.

[12]Arend, D.J., "Evaluation of an Innovative Supersonic Boundary Layer Transition Device - Phase I Results," AIAA-1998-3422, July 1998.

[13]Mani, M., J.A. Ladd, A.B. Cain, and R.H. Bush, "An Assessment of One- and Two-Equation Turbulence Models for Internal and External Flows," AIAA-1997-2010, July 1997.

[14]Spalart, P.R. and S.R. Allmaras, "A One-Equation Turbulence Model for Aerodynamic Flows," AIAA-1992-0439, January 1992.

[15]Menter, F.R., "Zonal Two-Equation k-ω Turbulence Models for Aerodynamic Flows," AIAA-1993-2906, July 1993.

[16]Mani, M. and D. Ota, "A Compressible Wall Function for Steady and Unsteady Flow Applications," AIAA-1999-3216, July 1999.

[17]Ladd, J.A. and M. Mani, "A Comparison of Steady State and Time Accurate CFD Methods for the Performance Prediction of a Transonic Pitot Inlet," AIAA-2004-0528, January 2004.

[18]Mayer, D.W. and Paynter, G.C., "Boundary Conditions for Unsteady Supersonic Inlet Analyses", *AIAA Journal*, Vol. 32, No. 6, 1994, pp. 1200-1206.

[19]Slater, J.W., "Verification Assessment of Flow Boundary Conditions for CFD Analysis of Supersonic Inlet Flows," AIAA-2001-3882, July 2001.